



ELSEVIER

Contents lists available at ScienceDirect

Applied Surface Science

journal homepage: www.elsevier.com/locate/apsusc

Full length article

Al₂O₃/Si_{0.7}Ge_{0.3}(001) & HfO₂/Si_{0.7}Ge_{0.3}(001) interface trap state reduction via in-situ N₂/H₂ RF downstream plasma passivation



Michael Breeden^a, Steven Wolf^a, Scott Ueda^a, Ziwei Fang^c, Chih-Yu Chang^c, Kechao Tang^d, Paul McIntyre^d, Andrew C. Kummel^{a,b,*}

^a Materials Science and Engineering Program, University of California, San Diego, La Jolla, CA 92093, United States

^b Department of Chemistry and Biochemistry, University of California, San Diego, La Jolla, CA 92093, United States

^c Taiwan Semiconductor Manufacturing Company, Ltd., Hsinchu City, Taiwan, Republic of China

^d Department of Materials Science and Engineering, Stanford University, Stanford, CA 94305, United States

ARTICLE INFO

Keywords:

Atomic layer deposition

Gate oxide

Silicon-germanium

Nitride passivation

Aluminum oxide

Hafnium oxide

ABSTRACT

A novel method for passivating the interface between Si_{0.7}Ge_{0.3} using an in-situ downstream RF plasma consisting of a nitrogen-rich mixture of H₂ and N₂ gases at 250 °C prior to atomic layer deposition (ALD) of Al₂O₃ and HfO₂ was demonstrated. XPS spectra of the interface with Al₂O₃ indicated the presence of a nitride layer enriched in SiON_x and depleted in Ge relative to the substrate. The electrical properties of this interface were characterized using I-V and variable frequency C-V measurements of MOS capacitors. The N₂/H₂ plasma passivation process produced a reduced density of interface trap states (D_{it}) and lower gate leakage compared with ex-situ HF clean and sulfur passivation for Al₂O₃ gate oxides. The lowered leakage current and D_{it} observed compared with HF(aq) or sulfur-passivated surfaces were consistent with enhanced oxide nucleation due to N₂/H₂ plasma passivation lowering carbon surface contamination and dangling bonds. TEM/EELS analysis of the interface was consistent with the presence of a thin interfacial nitride layer suppressing the formation of Ge–O bonds at the interface to form an SiO_x-rich interlayer (IL).

1. Introduction

To meet the demands of higher-performance, lower-power computing devices, the continued scaling of complementary metal-oxide-semiconductor (CMOS) devices requires the use of high-dielectric constant insulators (high-k dielectrics) and new channel materials. One promising class of channel materials are silicon-germanium (SiGe) alloys. The enhancement of hole mobility compared with Si due to splitting of the valence band heavy and light-hole band degeneracies makes tunable-Ge content SiGe channels desirable for use in p-type MOSFETs [1–3]. In comparison with other channel materials such as III–V compounds, SiGe alloys can be introduced into existing CMOS process flows, and growth of epitaxial SiGe layers by low-pressure chemical vapor deposition (LPCVD) or molecular beam epitaxy (MBE) has been well-studied and is in commercial use for heterojunction bipolar transistors, [4,5] as well as for stressor materials in strained-Si channel MOSFETs [6].

High-k dielectrics containing Al and/or Hf have been integrated successfully with commercial Si-channel CMOS processes since the 45 nm node [23,24]. On Si, the density of interfacial defects is low, and

attempts at improving the quality of the gate oxide have focused on the suppression of SiO₂ formation at the interface using a Ti- or La-doped HfO₂ dielectric to ensure an amorphous microstructure and formation of Hf-silicate at the interface to improve capacitance [25,26]. Conversely, formation of low defect interfaces between high-k oxides and higher-mobility channel materials such as GaAs or InGaAs has been challenged by high densities of defects with HfO₂, Al₂O₃, and TiO₂ gate oxides, or mixed metal oxides and silicates [27]. Chemical passivation of these surface defects prior to high-k deposition by ALD has been achieved on III–V substrates by employing thin Al₂O₃ layers to suppress As–O and Ga–O formation [28], as well as the use of dimethylaluminum hydride and O₂ in an MOCVD process to remove native oxides on InGaAs prior to deposition of HfTiO dielectric [29]. Suppression of an interfacial layer on the high-k/GaAs system has been achieved through nitrogen reactive sputtering of HfTi to form HfTiON [30]. In-situ plasma nitridation has also been reported on InGaAs using alternating pulses of N₂ plasma and trimethylaluminum prior to HfO₂ deposition [31]. Two-dimensional materials such as graphene offer the potential for zero interfacial layer thickness, but the chemically-inert surface of graphene has limited nucleation density of oxide layers. Nucleation of

* Corresponding author at: Materials Science and Engineering Program, University of California, San Diego, La Jolla, CA 92093, United States.

E-mail address: akummel@ucsd.edu (A.C. Kummel).

<https://doi.org/10.1016/j.apsusc.2019.01.216>

Received 1 September 2018; Received in revised form 22 January 2019; Accepted 23 January 2019

Available online 26 January 2019

0169-4332/ © 2019 Elsevier B.V. All rights reserved.

Al_2O_3 on graphene has been achieved by pre-pulsing H_2O prior to ALD, with physisorbed H_2O acting as a seed for subsequent reaction with trimethylaluminum (TMA) [35,36].

Passivation of interfacial defects on SiGe-channel CMOS devices requires a different approach than on III–V semiconductor channel devices. In-situ nitridation has been extensively studied on Ge MOS devices in suppressing the formation of thermally-unstable GeO_2 and diffusion of Ge into the high- k dielectric by terminating the surface with Ge nitrides and oxynitrides, resulting in high thermal stability and low interface state densities (D_{it}) [7–9]. However, the relative stability of Si–N bonds compared with Ge–N bonds has resulted in higher interface state defect densities for SiGe alloys. Low D_{it} values for SiGe have been reported by using post-deposition plasma nitridation by N_2 [10], passivation of SiGe by aqueous sulfur treatment [11], and NH_3 plasma nitridation [12]. However, post-deposition nitridation limits equivalent oxide thickness scaling and control over initial nucleation and growth, while aqueous sulfur passivation presents reliability concerns while requiring ex-situ treatment. NH_3 plasma nitridation, while successfully employed for plasma-enhanced ALD processes of metal nitrides, results in a fixed ratio of N and H species in plasma, which may result in suboptimal nitridation conditions for surface passivation [37].

This work demonstrates the use of a tunable mixture of H_2 and N_2 species in an RF downstream plasma to passivate the surface of SiGe prior to deposition of gate oxide. Capacitance-voltage and current-voltage measurements were used to determine the effectiveness of the N_2/H_2 RF plasma process on the interface state density and leakage current, while X-ray photoelectron spectroscopy (XPS), transmission electron microscopy (TEM), and electron energy-loss spectroscopy (EELS) were employed to investigate the chemical environment of the SiGe/high- k interface, as well as the interfacial layer thickness and composition using Al_2O_3 and HfO_2 as gate dielectrics.

2. Experimental

In this study, to demonstrate the effectiveness of the N_2/H_2 downstream plasma passivation method, metal-oxide-semiconductor capacitors (MOSCAPs) were fabricated with Al_2O_3 and HfO_2 dielectrics on a $\text{Si}_{0.7}\text{Ge}_{0.3}$ channel with (001) orientation. The SiGe channel layer consisted of a 9-nm-thick p-type $\text{Si}_{0.7}\text{Ge}_{0.3}$ (001) layer with $1 \times 10^{18} \text{ cm}^{-3}$ dopant density epitaxially grown on p-type Si(001) by molecular beam epitaxy (Applied Materials, Inc.). Prior to dielectric deposition, each sample underwent an organic clean via a rinse of acetone, methanol, and DI H_2O , followed by native oxide removal via 2.5 cycles of 1 minute immersion in 2% HF(aq) and 1 minute immersion in DI H_2O , following the method of Oshima et al., on high-Ge content substrates [7]. To benchmark N_2/H_2 plasma passivation in comparison with other methods, three methods were compared – HF(aq) only clean in which no further preparation prior to dielectric deposition was performed, ex-situ sulfur passivation in which the sample was immersed in a 25% solution of $(\text{NH}_4)_2\text{S}$ for 15 min, and in-situ N_2/H_2 plasma pre-deposition. After ex-situ sample preparation, samples were transferred to the ALD chamber within 2 min to minimize air exposure.

Fig. 1 depicts the chamber used to perform dielectric deposition and in-situ plasma passivation. The main deposition chamber is pumped to a base pressure of 2×10^{-2} Torr via rotary vane mechanical pump and is connected to a load lock for sample transfer. Above the chamber, an RF downstream plasma source (PIE Scientific, Inc.) was mounted to generate the N_2/H_2 plasma mixture. A sapphire plasma tube was employed to resist attack from atomic H generated in the plasma [13]. An ultra-high purity mixture of N_2 and 5% H_2 in Ar (Praxair) at 1 Torr pressure was employed for the plasma source with an N-to-H ratio of 20:1, which was maintained at an RF power of 20 W. Plasma processing was performed after the sample was pre-heated for 5 min at 250 °C.

For ALD of the dielectric layer, trimethylaluminum (TMA, Strem Chemicals, Inc.), tetrakis(dimethylamino) hafnium (TDMAH, Strem Chemicals, Inc.), and 18 M Ω ·cm DI H_2O were mounted to the chamber

for Al_2O_3 and HfO_2 deposition. TMA and H_2O sources were kept at 25 °C, while the TDMAH source was heated to 70 °C. All chamber walls, precursor dosing lines, and pump lines were held at a temperature of 130 °C to ensure precursors would not condense on the wall prior to reaching the sample and to minimize powder formation. To maintain the deposition temperature at 250 °C, a UHV pedestal heater (Heatwave Labs, Inc.) was utilized, and samples were pre-heated for 5 min prior to in-situ processing. Pneumatic valves controlled via custom LabVIEW program were employed to control dosing times of precursors. Expansion volume dosing was used for TMA and H_2O dosing due to their high vapor pressures. During Al_2O_3 cycles, TMA was dosed into the expansion volume for 600 ms, followed by a 5 s dose to the chamber and 1 s inert purge. Subsequently, water was dosed into the expansion volume for 700 ms, followed by a 5 s dose and 1 s inert purge. For HfO_2 cycles, TDMAH was dosed directly to the chamber for 250 ms, followed by a 25 s inert purge, and the water half-cycle was dosed to the expansion volume for 600 ms, dosed to the chamber for 5 s and inert purge for 10 s. The TDMAH and H_2O purge times were increased to avoid the possibility of gas-phase reactions inducing CVD, as the lower vapor pressure of the TDMAH precursor resulted in incomplete gas evacuation before the next half-cycle without extension. A constant 100 mTorr UHP N_2 (Praxair) purge was run during deposition to prevent mixing of precursors in the reaction chamber.

To complete the MOSCAP structure, 30 nm of Ni was thermally evaporated to form 150 μm diameter circular gates, and a backside 100 nm Al contact was deposited via DC sputtering. After fabrication, MOSCAPs were annealed in forming gas (5% H_2 , 95% N_2) at 300 °C for 15 min, 330 °C for 10 min, and 350 °C for 5 min, following the method described by Kavrik et al. [32]. Capacitance-, conductance- and current-voltage (C-V/G-V/I-V) characteristics of the MOSCAPs were performed using an Agilent B1500 semiconductor analyzer with an AC modulation amplitude of 30 mV between a gate bias of -2 and $+2$ V at frequencies from 2 kHz to 1 MHz. Using the C-V and G-V relationships measured, interface state densities (D_{it}) were measured using both the conductance method [14] and the full interface state distribution and density of bulk-oxide trap states was calculated using the method of Chen and Yuan [15,16]. The gate leakage current was measured between -2 and $+2$ V bias.

To investigate the chemical environment at the high- k /SiGe interface, 5 cycles of Al_2O_3 were deposited on SiGe samples after organic and HF pre-clean, and with or without N_2/H_2 plasma passivation. These samples were removed and rapidly transferred (with a maximum of 2 min of air exposure) to a surface analysis tool consisting of load lock and UHV chamber at a base pressure of 1×10^{-10} Torr with a monochromatic XM1000 MkII/SPHERA XPS system (Omicron Nanotechnology GmbH) for collection of XPS spectra. The source used was a monochromatic Al $K\alpha$ source at 1486.7 eV with an analyzer pass energy of 50 eV and linewidth of 0.1 eV, and XPS spectra were collected at 30° with respect to parallel to the sample. XPS analysis was performed using CASA XPS 2.3 software, with raw peak areas corrected via Schofield photoionization cross-sectional relative sensitivity factors. Elemental analysis of the high- k /SiGe interface was performed using TEM/EELS at electron acceleration of 80 keV to minimize beam damage to the Al_2O_3 layer. Principal component analysis was used to de-noise EELS spectra [17].

3. Results & discussion

3.1. $\text{Al}_2\text{O}_3/\text{SiGe}$

To compare the effects of N_2/H_2 plasma passivation with HF(aq) only clean and sulfur passivation, 40 ALD cycles of Al_2O_3 were deposited at 250 °C and MOSCAPs were fabricated. Fig. 2 displays the C-V characteristics of three of the devices, with the HF(aq) only cleaned sample exhibiting a larger low-frequency “bump” between 0 and 0.5 V gate bias than either the N_2/H_2 plasma passivated surface or the sulfur-

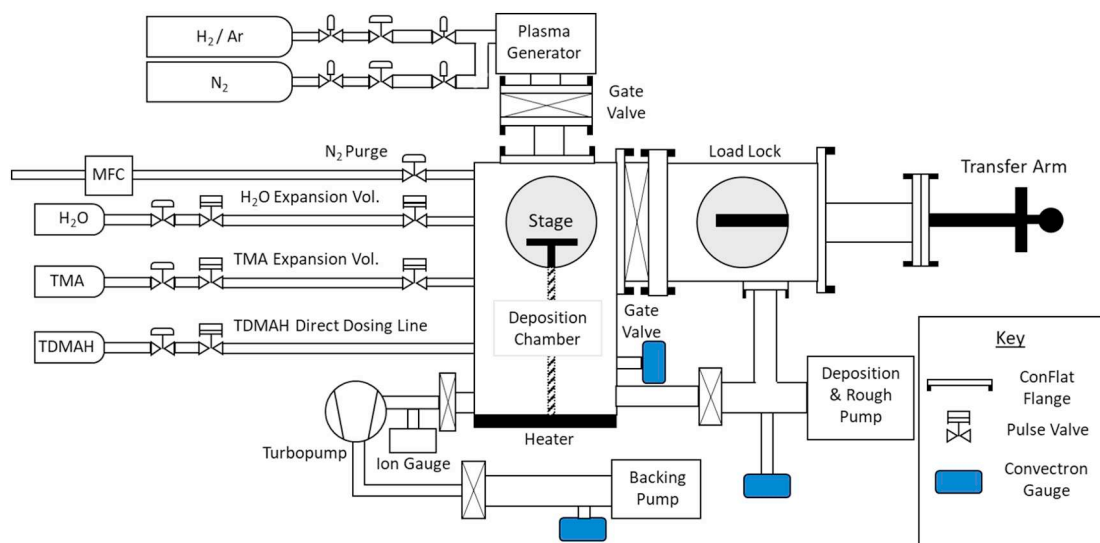


Fig. 1. Chamber schematic showing the load-locked deposition chamber with attached RF downstream plasma source, heated sample stage, and precursor dosing lines.

passivated surface. By the conductance model [14], interface state densities were found to be 3.6×10^{12} , 8.9×10^{11} , and $7.2 \times 10^{11} \text{ cm}^{-2} \text{ eV}^{-1}$ at midgap for HF only, HF + ex-situ sulfur, and HF + in-situ N_2/H_2 plasma passivation, respectively. The in-situ N_2/H_2 plasma passivation D_{it} is comparable to the peak value obtained by post-deposition plasma nitridation and demonstrates a factor of 3 improvement in interface state density over in-situ ammonia plasma nitridation [10,12]. Oxide capacitances derived from the full interface state model were 1.02, 1.13, and $1.10 \mu\text{F/cm}^2$, respectively [15]. Equivalent oxide thickness (EOT) for the three Al_2O_3 devices was 3.4, 3.1, and 3.1 nm. The sulfur-cleaned and N_2/H_2 plasma-cleaned samples exhibited similar oxide capacitances, illustrating that the N_2/H_2 plasma passivation technique is effective in preventing unwanted interfacial oxide growth during Al_2O_3 ALD.

Fig. 3 shows the leakage current density and interface state density as a function of energy across the bandgap for the three devices as derived by the Chen full interface state model. Integrated interface state densities across the bandgap were $1.5 \times 10^{12} \text{ cm}^{-2}$ for the HF(aq) only sample, $3.4 \times 10^{11} \text{ cm}^{-2}$ for the HF(aq) + ex-situ sulfur-passivated sample, and $2.4 \times 10^{11} \text{ cm}^{-2}$ for the HF(aq) + in-situ N_2/H_2 plasma-passivated sample. The peak of the interface state density is located at 0.2 to 0.5 eV above the valence band edge for all three devices. The energy range of this interface state density peak corresponds with that of the peak interface state density reported for the Si/SiO₂ interface, which was found to be due to the formation of dangling bonds at Si P_b centers acting as amphoteric

defects [17,18]. By comparison, interface states at the Ge/GeO₂ interface have been found to act as acceptors, and observed interface state densities are consistent with GeO_x-induced defects in the oxide interfacial layer [19–21]. This result is consistent with the formation of Si-O-Al bonds at the interface which are effectively passivated by hydrogen after forming gas anneal. Border trap densities (N_{bt}) were calculated with the model of Yuan, with N_{bt} values for HF only, HF + sulfur, and HF + plasma passivated devices being $3.9 \times 10^{19} \text{ cm}^{-3} \text{ eV}^{-1}$, $1.8 \times 10^{19} \text{ cm}^{-3} \text{ eV}^{-1}$, and $1.8 \times 10^{19} \text{ cm}^{-3} \text{ eV}^{-1}$, respectively [16]. Care in interpreting these values should be taken, as the model does not consider substrate series-resistance or correct for the effect of gate leakage current density [16].

The effect of the forming gas anneal on the plasma-cleaned devices is illustrated in Fig. 4. The temperatures and times used for the forming gas anneal were chosen after an optimization of anneal conditions, from which it was found that a ramped temperature anneal from 300 °C to 350 °C for 30 min improved the interface quality over a constant temperature anneal, following the method of Kavrik et al. [34]. This is reflected in the reduction in D_{it} from $3.6 \times 10^{12} \text{ cm}^{-2} \text{ eV}^{-1}$ for the HF (aq)-only sample before anneal, to $1.1 \times 10^{12} \text{ cm}^{-2} \text{ eV}^{-1}$ for the 15 min 300 °C annealed sample and $7.2 \times 10^{11} \text{ cm}^{-2} \text{ eV}^{-1}$ for the 30 min ramped forming gas anneal. It is hypothesized that the interfacial defects as reflected in the conductance-voltage characteristics have a distribution of activation energies and preexponential factors; ramping the temperature of anneal over time, these defects can be more effectively passivated while minimizing the total thermal budget

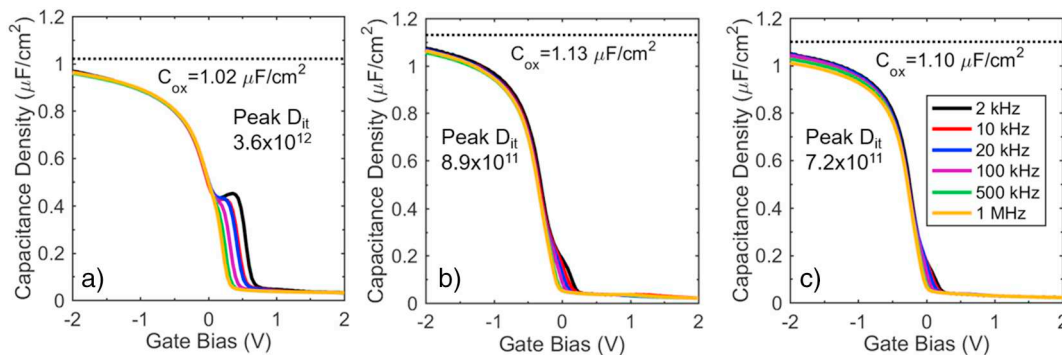


Fig. 2. 2 kHz–1 MHz C-V characteristics of 40 cycle Ni/ $\text{Al}_2\text{O}_3/\text{Si}_{0.7}\text{Ge}_{0.3}$ MOSCAPs after forming gas anneal. (a) HF(aq) pre-clean only – 5.9 nm oxide + interlayer thickness (b) HF(aq) clean + ex-situ $(\text{NH}_4)_2\text{S}$ treatment – 6.1 nm oxide + interlayer thickness (c) HF(aq) clean + N_2/H_2 plasma treatment – 6.0 nm oxide + interlayer thickness. C_{ox} values were estimated using quasi-static C-V simulations.

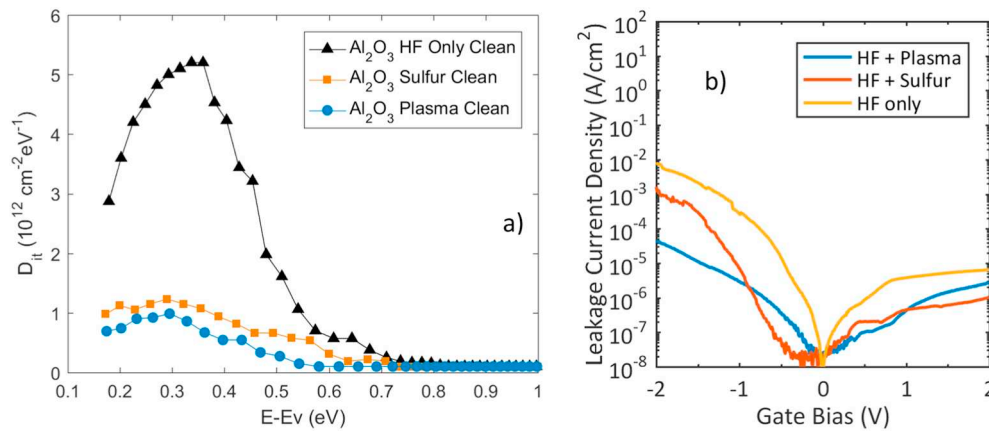


Fig. 3. (a) Full interface state model [15] and (b) I-V characteristics of 40 cycle Ni/Al₂O₃/Si_{0.7}Ge_{0.3} MOSCAPs after forming gas anneal.

extended, limiting Ge diffusion through the interface during anneal.

To evaluate the chemical structure of the interface between Al₂O₃ and SiGe, 5 cycles of Al₂O₃ were deposited on SiGe at 250°C. Prior to deposition, samples were cleaned with HF(aq) only or with HF(aq) + in-situ N₂/H₂ RF plasma passivation to compare the effectiveness of the passivation techniques. XPS spectra for a) Si 2p, b) Ge 3d, c) N 1s, and d) O 1s are shown in Fig. 5, and the integrated XPS spectrum area of each peak and the SiON_x and GeON_x peaks are shown in Fig. 5(e). The composition of the nitride peaks corresponding to SiN_x and GeN_x components are observed at 102.1 eV and 31.8 eV, respectively, for the N₂/H₂ plasma-passivated surface. The N 1s peak is absent from the HF only cleaned sample, reflecting the lack of nitrogen treatment, while on the N₂/H₂ plasma cleaned sample, the peak is centered at 398.0 eV, consistent with values reported previously for SiON_x [32,33].

The ratio of the nitride signal to the elemental XPS peak is approximately 39% for the Si peak and 17% for the Ge peak on the plasma-passivated surface, suggesting preferential formation of Si–N bonds over Ge–N bonds. This is consistent with previous XPS studies of preferential formation of Si₃N₄ compared with Ge₃N₄ and is consistent with the higher heat of formation for Si₃N₄ at –744 kJ/mol compared with –63 kJ/mol for Ge₃N₄. Due to the lower Ge₃N₄ heat of formation, only a small component of stoichiometric Ge oxynitride within the SiON_x layer is observed [22]. The resulting SiON_x-rich layer is more thermally stable and more likely to inhibit H₂O and Ge diffusion through the interface during ALD oxide growth, improving interface quality compared with HF(aq) only cleaned interfaces [33].

Furthermore, a small GeO_x shoulder on the Ge peak located at 30.5 eV is observed on the HF(aq) only cleaned sample, while the N₂/H₂ plasma passivated sample lacks this feature. This is also consistent with the suppression of Ge–O bonding in the nitrated sample. The intensity of the Si and Ge peaks is suppressed for the N₂/H₂ plasma-passivated surface compared with the surface cleaned only by HF(aq) prior to deposition, suggesting a thicker layer of Al₂O₃. This is consistent with the N₂/H₂ plasma passivation enhancing initial nucleation of the gate dielectric, which is reflected in the plasma-passivated devices exhibiting lower leakage currents.

The formation of the nitride interfacial layer is hypothesized to be due to the reaction of NH_x-radicals at the surface of the SiGe channel. A plasma power of 20 W is sufficient to ionize N₂ and H₂, but since the pressure in the chamber exceeds 1 mTorr, ion recombination of these species occurs before the plasma gases can reach the surface of the sample. Instead, it is expected that atomic N formed in the plasma reacts with Si and Ge to form SiN_x and GeN_x, while the NH_x-radicals react with surface defect sites and C contamination on the surface. Previous studies of plasma nitridation on SiGe with ammonia have hypothesized the nitridation species to be atomic N, while residual carbon defects on the surface are cleaned up through reaction with NH_x radicals [10,12]. A higher N-to-H ratio is then expected to promote atomic N in the plasma gases, enhancing surface nitridation.

To investigate the thickness of the interfacial layer and the chemical structure of the interface in a full MOSCAP device after forming gas anneal, high-resolution transmission electron microscopy (HRTEM) was used to image a cross section of the interface. Additionally, electron

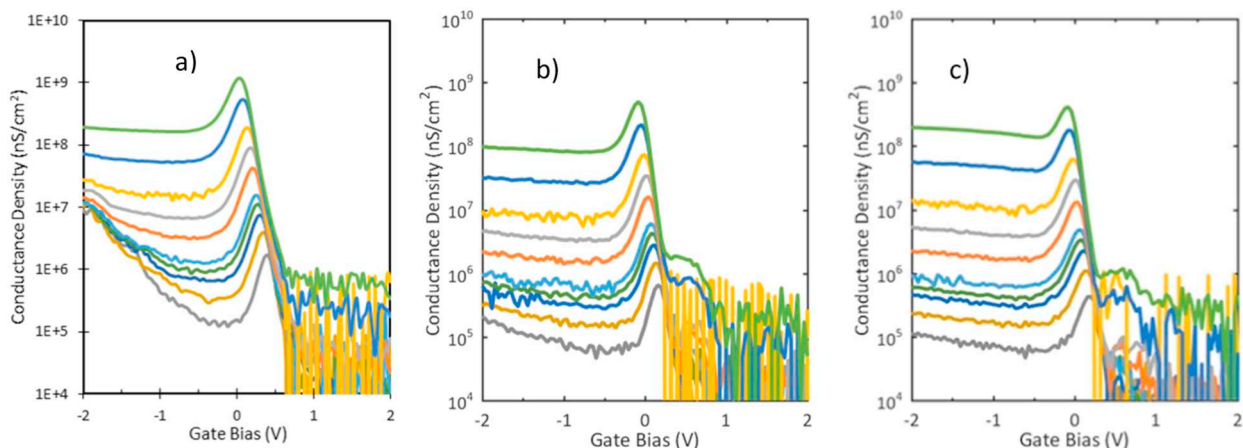


Fig. 4. Conductance-voltage characteristics of Ni/Al₂O₃/Si_{0.7}Ge_{0.3} MOSCAPs with 40 cycles of Al₂O₃ ALD after N₂/H₂ plasma passivation (a) before ramped forming gas anneal, (b) after 15 min 300 °C forming gas anneal, and (c) after 30 min ramped forming gas anneal from 300 to 330 to 350 °C.

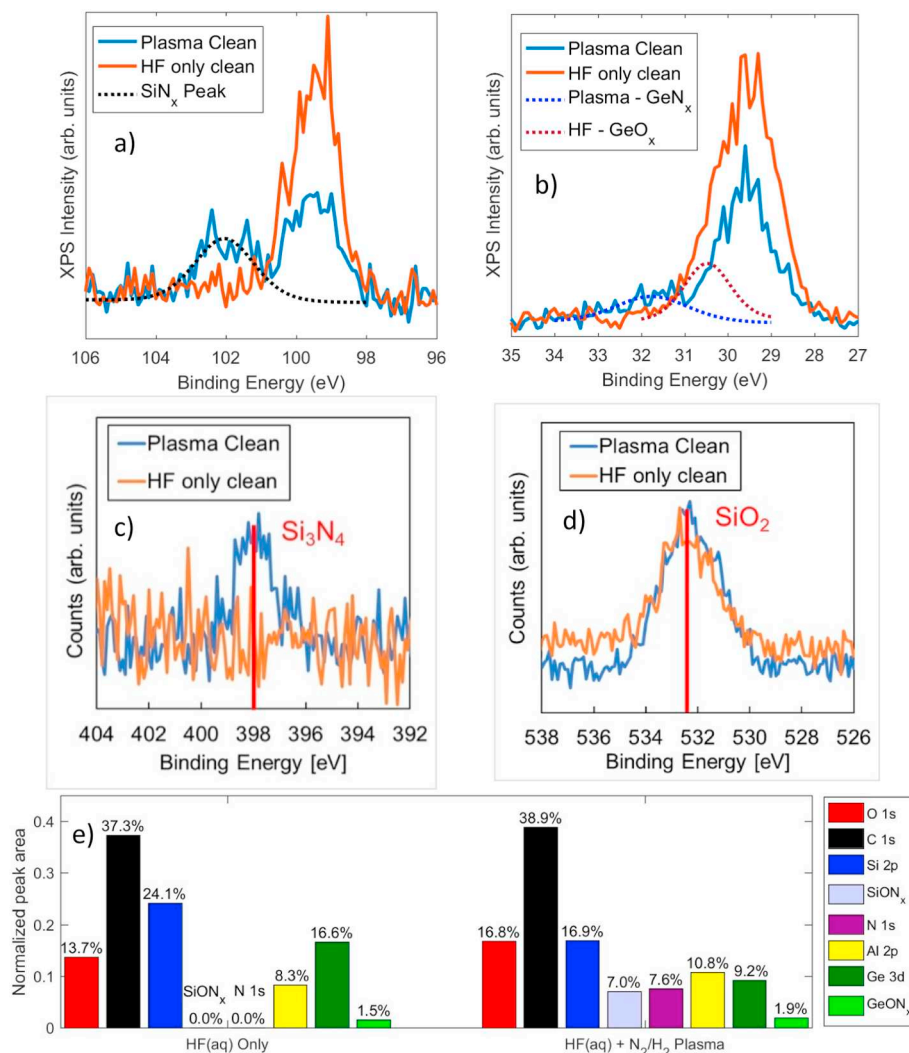


Fig. 5. XPS spectra for (a) Si 2p peak (b) Ge 3d peak (c) N 1s peak (d) and O 1s peak for 5 cycles of Al₂O₃/Si_{0.7}Ge_{0.3}. (e) Normalized XPS integrated signal values for HF(aq) only and HF(aq) + N₂/H₂ plasma passivated SiGe.

energy-loss spectroscopy (EELS) was employed to capture the chemical structure of the interface on the HF(aq) only, sulfur-passivated, and N₂/H₂ plasma passivated devices. Fig. 6 shows HRTEM and EELS spectra across the gate stack on the HF(aq) only, sulfur-passivated, and N₂/H₂ passivated devices. From inspection of the HRTEM and EELS data, the interfacial layer thickness of the plasma-cleaned device was 1.5 nm, compared with 1.3 nm for the sulfur cleaned device and 1.6 nm for the HF(aq) only cleaned device. However, the nonuniformity of the interfacial thickness suggests no correlation of interfacial thickness with improved interfacial quality. Fig. 5f contains the EELS data for the sample passivated by N₂/H₂ plasma, which illustrates a nitride layer 1.5 nm thick at the interface. At the center of the N peak, the ratio of Ge relative to Si is 0.14, which is consistent with an interlayer mostly consisting of SiON_x with low Ge content relative to the HF(aq) only cleaned surface. This suggests that the nitride formed during plasma-passivation is effective in suppressing the formation of Ge–O bonds by preventing the diffusion of Ge through to the gate oxide during growth.

3.2. HfO₂/SiGe

To determine if the N₂/H₂ plasma passivation is effective in passivating the interface between SiGe and a higher-dielectric constant

insulator, MOSCAPs with 40 and 50 ALD cycles of HfO₂ were fabricated. Fig. 7 illustrates the C-V characteristics of five of these devices, with the HF(aq) only clean exhibiting a larger low-frequency “bump” between 0 and 0.5 V gate bias than the N₂/H₂ plasma passivated surface. Unlike the Al₂O₃ MOSCAPs, sulfur passivation of the HfO₂ MOSCAPs was unsuccessful in yielding devices with lower leakage and defect densities than the HF(aq) only device, and 40 cycle MOSCAPs prepared by HF(aq) only clean had a leakage current density too large to accurately extract the interface state density profile from the measured C-V data. Furthermore, while interface state analysis was performed for the 40 cycle sulfur-passivated device, the high leakage current density may call into question the validity of the extracted profile. It is noted that the poor performance of the sulfur passivated HfO₂ MOSCAPs may be deposition system and precursor specific. By the conductance model, interface state densities for the 40 cycle HfO₂ devices were found to be 6.1×10^{12} , 4.9×10^{12} , and $3.8 \times 10^{12} \text{ cm}^{-2} \text{ eV}^{-1}$ at midgap for the HF(aq) only, HF(aq) + ex-situ sulfur, and HF(aq) + in-situ N₂/H₂ plasma passivation, respectively. For the 50 cycle devices, the HF(aq) only cleaned device had a D_{it} of $4.8 \times 10^{12} \text{ cm}^{-2} \text{ eV}^{-1}$, while the HF(aq) + N₂/H₂ plasma-passivated device had a D_{it} of $2.9 \times 10^{12} \text{ cm}^{-2} \text{ eV}^{-1}$. Oxide capacitances derived from the full interface state model were 1.90, 1.85, and 2.48 $\mu\text{F} \cdot \text{cm}^{-2}$

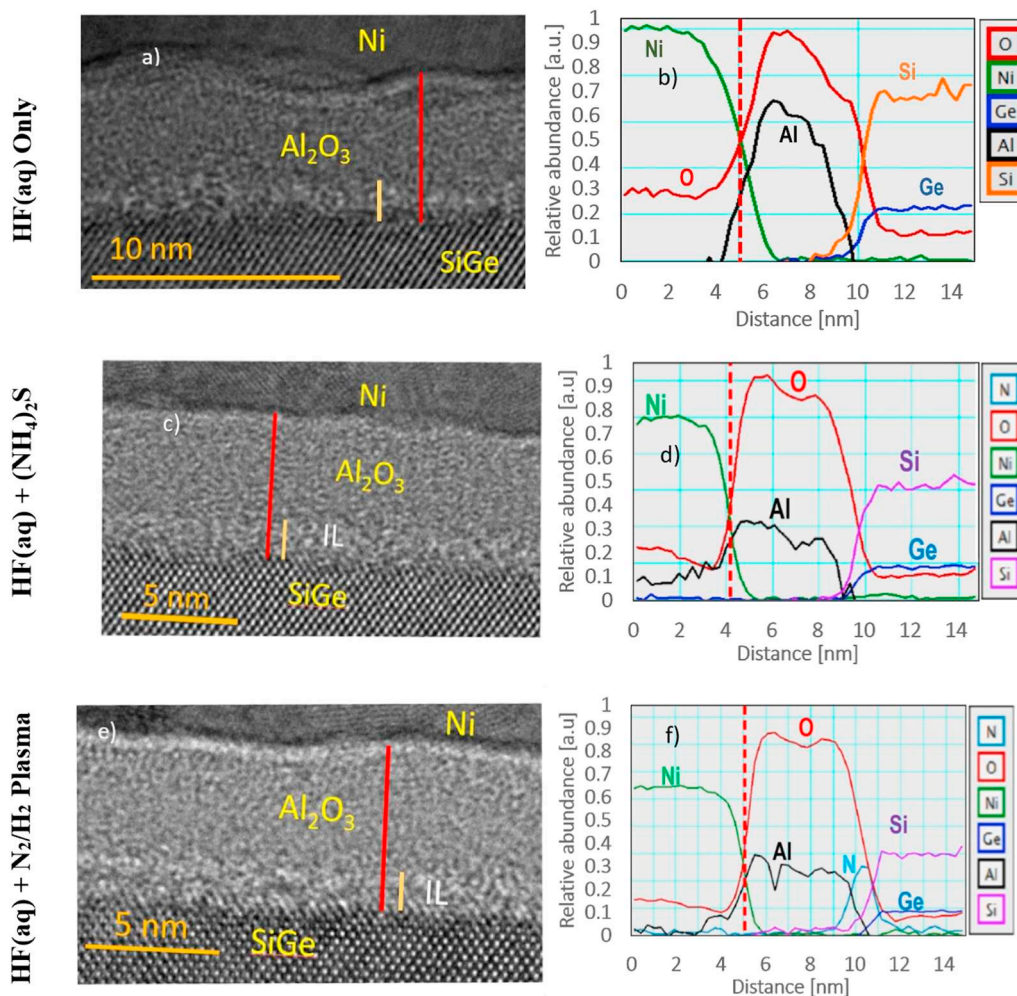


Fig. 6. (a) HRTEM of Al₂O₃/SiGe MOSCAP treated with 2% HF(aq) pre-deposition, (b) EELS spectrum line trace of Al₂O₃/SiGe treated with 2% HF(aq) pre-deposition, (c) HRTEM of Al₂O₃/SiGe MOSCAP passivated by aqueous sulfur pre-deposition, (d) EELS spectrum line trace of Al₂O₃/SiGe passivated by aqueous sulfur pre-deposition, (e) HRTEM of Al₂O₃/SiGe MOSCAP passivated by N₂/H₂ plasma pre-deposition, (f) EELS spectrum line trace of Al₂O₃/SiGe passivated by N₂/H₂ plasma pre-deposition.

for the 40 cycle devices, and 1.95 and 2.14 $\mu\text{F}\cdot\text{cm}^{-2}$ for the 50 cycle devices, respectively, demonstrating that an improvement in the interface state density through the N₂/H₂ plasma passivation technique can also be extended to higher dielectric constant materials than Al₂O₃, yielding a lower equivalent oxide thickness.

Fig. 8 details the interface state density across the bandgap and leakage current characteristics for 40 and 50 cycle HfO₂ MOSCAPs. Comparing the leakage current at -2 V bias for 40 cycle HfO₂ MOSCAPs, a 10,000 \times reduction in leakage is observed for the N₂/H₂ plasma passivated device after forming gas anneal, compared with the HF(aq) only cleaned device. This is indicative of a significant improvement in oxide nucleation and growth on the nitrated interfacial layer. The full interface state model developed by Chen et al. was applied to HfO₂ MOSCAPs with lower leakage to characterize the integrated interface state density across the bandgap [15]. The 50 cycle HF(aq) only sample had an integrated interface state density across the bandgap of $1.6 \times 10^{12}\text{ cm}^{-2}$, while the 50 cycle N₂/H₂ plasma passivated sample had an integrated interface state density of $8.0 \times 10^{11}\text{ cm}^{-2}$, a 2 \times improvement. The 40 cycle HF(aq) + ex-situ sulfur-passivated sample had an integrated interface state density of $1.2 \times 10^{12}\text{ cm}^{-2}$, and the 40 cycle N₂/H₂ plasma-passivated sample $1.1 \times 10^{12}\text{ cm}^{-2}$. Integrated interface state density is significantly higher than that of Al₂O₃ MOSCAPs, which is consistent with poor diffusion barrier properties of

deposited HfO₂ compared with Al₂O₃. It is hypothesized that the higher integrated D_{it} for the 40 cycle vs 50 cycle ALD processes are consistent with HfO₂ being a poorer diffusion barrier for the ex-situ transfer for metal gate deposition than Al₂O₃. Finally, border-trap densities (N_{bt}) were calculated for the non-leaky devices, as the 40 cycle HF only and 50 cycle HF + sulfur passivated devices were too leaky for a meaningful model fit. The 50 cycle HF only device had an N_{bt} of $3.3 \times 10^{19}\text{ cm}^{-3}\text{ eV}^{-1}$, while the 40 cycle HF + sulfur passivated device had an N_{bt} of $6.0 \times 10^{19}\text{ cm}^{-3}\text{ eV}^{-1}$. Conversely, the 40 and 50 cycle HF + plasma-passivated devices had N_{bt} values of $1.3 \times 10^{19}\text{ cm}^{-3}\text{ eV}^{-1}$ and $1.1 \times 10^{19}\text{ cm}^{-3}\text{ eV}^{-1}$. Under the border trap model developed by Yuan et al., a single border trap state is assumed and series resistance is neglected, yet these results are still consistent with effective oxide nucleation at the plasma-passivated interface decreasing tunneling into oxide trap states close to the interface [16].

TEM and EELS were used to characterize the thickness and chemical composition of the interfacial layer for the HfO₂ MOSCAPs. Fig. 9 shows the HRTEM images and EELS data for the HF(aq) only, sulfur, and N₂/H₂ plasma passivated devices. The interfacial layer thickness of the plasma-cleaned device was 1.3 nm compared with 1.2 nm for the sulfur cleaned device, and 1.4 nm for the HF(aq) only device. Similar to the Al₂O₃ MOSCAPs, the ratio of Ge to Si in the interface is observed to

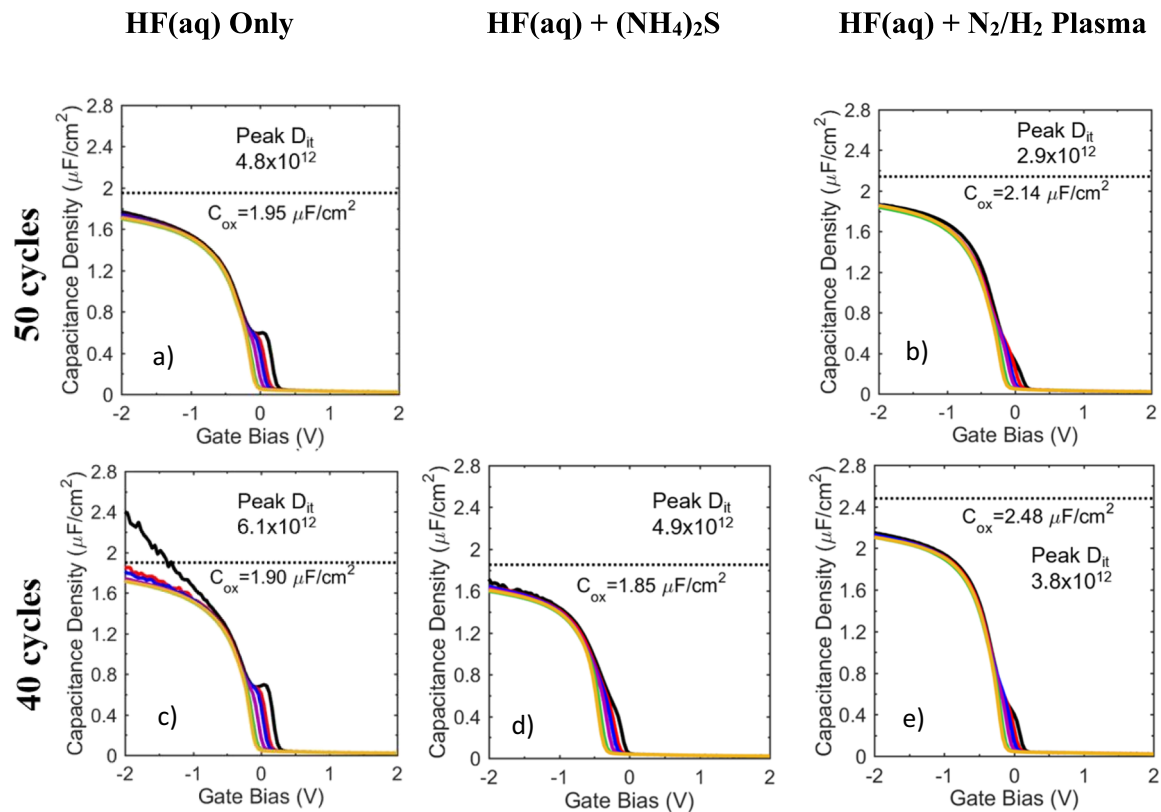


Fig. 7. 2 kHz–1 MHz C-V characteristics of 40 and 50 cycle Ni/HfO₂/Si_{0.7}Ge_{0.3} MOSCAPs after forming gas anneal. (a) HF(aq) pre-clean only, 50 cycles ALD (b) HF (aq) clean + N₂/H₂ plasma treatment, 50 cycles ALD (c) HF(aq) pre-clean only, 40 cycles ALD (d) HF(aq) clean + ex-situ (NH₄)₂S treatment, 40 cycles ALD (e) HF (aq) + N₂/H₂ plasma treatment, 40 cycles ALD. C_{ox} values were estimated using quasi-static C-V simulations.

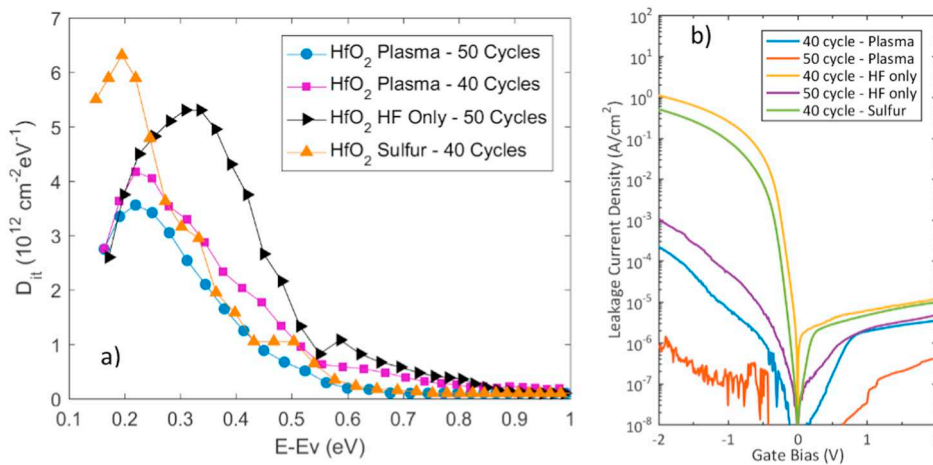


Fig. 8. (a) Full interface state model [15] and (b) I-V characteristics of 40 and 50 cycle Ni/HfO₂/Si_{0.7}Ge_{0.3} MOSCAPs after forming gas anneal.

decrease relative to the SiGe layer for the N₂/H₂ plasma passivated devices compared with the HF(aq) only devices, with the ratio of Ge to Si at the middle of the interfacial layer being 0.16 for the plasma-passivated device compared with 0.35 for the HF(aq) only device and 0.26 for the sulfur-passivated device. Additionally, the Ge content falls off 0.4 nm than the Si content in the HF(aq) only device, suggesting that the HF(aq) treated surface causes the interlayer on HfO₂ to be a poorer diffusion barrier for Ge compared with plasma and sulfur passivation. The maximum of the N peak observed in Fig. 9f corresponds to a region with lower Ge content relative to Si and significant oxygen, consistent with an interlayer consisting of mostly SiO_xN_x.

4. Conclusion

An in-situ, tunable mixture of N and H in an RF downstream plasma has been demonstrated to effectively passivate the surface of SiGe prior to deposition of high-k gate dielectrics Al₂O₃ and HfO₂. As opposed to ex-situ aqueous sulfur-containing treatment or post-deposition plasma nitridation, the pre-deposition in-situ nitridation by N₂/H₂-containing plasma reduces interfacial trap state density by 80% compared with HF (aq) only treatment, and by 20% compared with aqueous sulfur passivation. Investigation of the interfacial composition carried out by XPS illustrates that the formation of an SiO_xN_y interfacial layer both

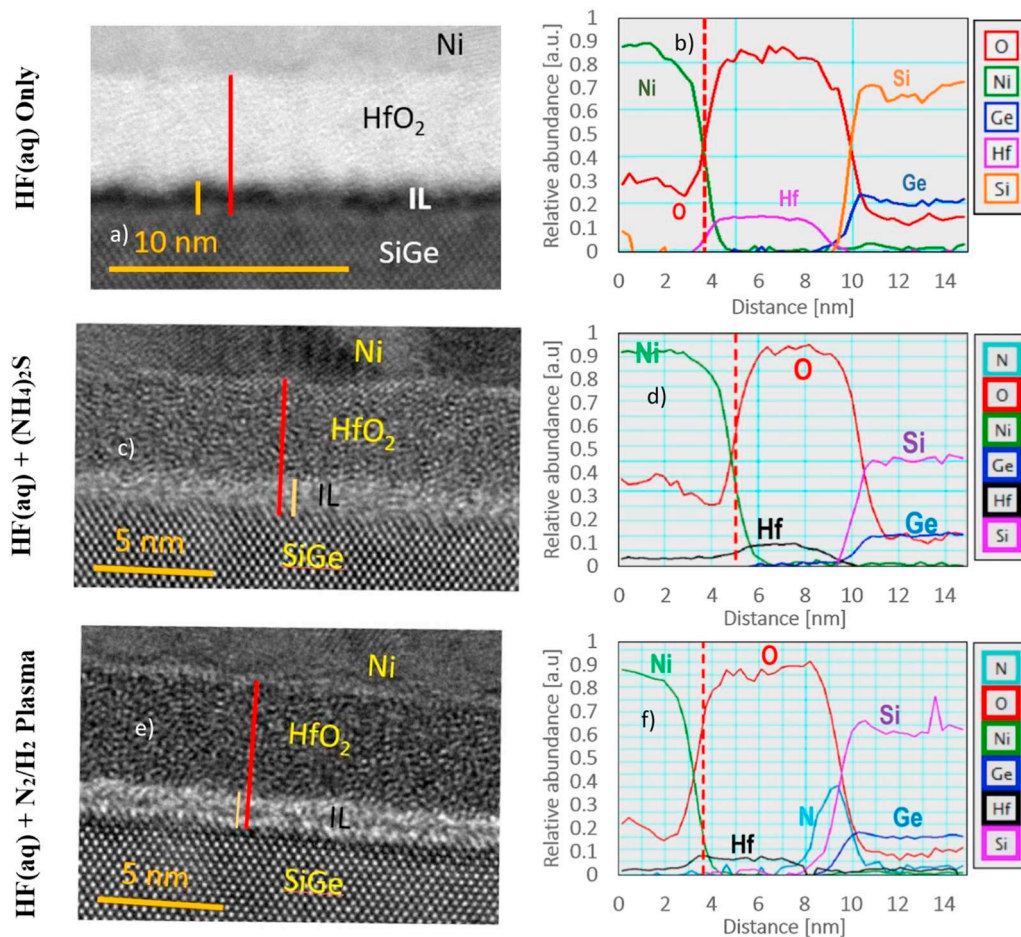


Fig. 9. (a) HRTEM of HfO₂/SiGe MOSCAP treated with 2% HF(aq) pre-deposition, (b) EELS spectrum line trace of HfO₂/SiGe treated with 2% HF(aq) pre-deposition, (c) HRTEM of HfO₂/SiGe MOSCAP passivated by aqueous sulfur pre-deposition, (d) EELS spectrum line trace of HfO₂/SiGe passivated by aqueous sulfur pre-deposition, (e) HRTEM of HfO₂/SiGe MOSCAP passivated by N₂/H₂ plasma pre-deposition, (f) EELS spectrum line trace of HfO₂/SiGe passivated by N₂/H₂ plasma pre-deposition.

decreases D_{it} and lowers leakage currents, which is consistent with an enhancement in gate oxide nucleation. TEM/EELS analysis illustrates that this interfacial nitride layer is effective in suppressing the presence of Ge–O bonds in the interface.

Acknowledgements

This work was performed in part at the San Diego Nanotechnology Infrastructure (SDNI) of UCSD, a member of the National Nanotechnology Coordinated Infrastructure, which is supported by the National Science Foundation (Grant ECCS-1542148). Wafers were supplied by Applied Materials, Inc. This work was partially supported by gifts from Applied Materials, Inc. and Taiwan Semiconductor Manufacturing Company, Ltd.

Appendix A. Supplementary data

Supplementary data to this article can be found online at <https://doi.org/10.1016/j.apsusc.2019.01.216>.

References

- M.V. Fischetti, S.E. Laux, Band structure, deformation potentials, and carrier mobility in strained Si, Ge, and SiGe alloys, *J. Appl. Phys.* 80 (1996) 2234.
- C.W. Liu, M. Östling, J.B. Hannon, New materials for post-Si computing, *MRS Bull.* 39 (8) (2014) 658.
- O. Weber, et al., Fabrication and mobility characteristics of SiGe surface channel pMOSFETs with a HfO₂/TiN gate stack, *IEEE Trans. Electron Devices.* 53 (3) (2006) 449.
- A. Prujimboom, et al., Heterojunction bipolar transistors with SiGe base grown by molecular beam epitaxy, *IEEE Electron Device Lett.* 12 (7) (1991) 357.
- J.-M. Hartmann, et al., Effects of temperature and HCl flow on the SiGe growth kinetics in reduced-pressure chemical vapor deposition, *J. Vac. Sci. Technol. B.* 21 (6) (2003) 355.
- T. Ghani, et al., A 90 nm high volume manufacturing logic technology featuring novel 45 nm gate length strained silicon CMOS transistors, *IEDM Tech Dig.*, 2003, p. 11.6.1.
- Y. Oshima, et al., Chemical bonding, interfaces, and defects in hafnium oxide/germanium oxynitride gate stacks on Ge(100), *J. Electrochem. Soc.* 155 (12) (2008) G304.
- P. Bhatt, et al., Germanium oxynitride gate interlayer dielectric formed on Ge(100) using decoupled plasma nitridation, *Appl. Phys. Lett.* 103 (2013) 172107.
- N. Lu, et al., Ge diffusion in Ge metal oxide semiconductor with chemical vapor deposition HfO₂ dielectric, *Appl. Phys. Lett.* 87 (2005).
- J. Han, et al., Reduction in interface trap density of Al₂O₃/SiGe gate stack by electron cyclotron resonance plasma post-nitridation, *Appl. Phys. Express* 6 (2013) 051302.
- K. Sardashti, et al., Sulfur passivation for the formation of Si-terminated Al₂O₃/SiGe (001) interfaces, *Appl. Surf. Sci.* 366 (2016) 455.
- K. Sardashti, et al., Nitride passivation of the interface between high-k dielectrics and SiGe, *Appl. Phys. Lett.* 108 (2016) 011604.
- N.M. Johnson, et al., Hydrogen incorporation in silicon thin films deposited with a remote hydrogen plasma, *Appl. Phys. Lett.* 54 (2008) 1872.
- E.H. Nicollian, A. Goetzberger, The Si-SiO₂ interface – electrical properties as determined by the metal-insulator-silicon conductance technique, *Bell Syst. Tech. J.* 46 (1967) 1055.
- H.P. Chen, et al., Interface-state modeling of Al₂O₃-InGaAs MOS from depletion to inversion, *IEEE Trans. Electron Devices* 59 (2012) 2383.
- Y. Yuan, et al., A distributed bulk-oxide trap model for Al₂O₃ InGaAs MOS devices, *IEEE Trans. Electron Devices* 59 (2012) 2100.
- M. Bosman, et al., Mapping chemical and bonding information using multivariate analysis of electron energy-loss spectrum images, *Ultramicroscopy* 106 (11) (2006) 1024.

- [18] E.H. Poindexter, et al., Electronic traps and P_b centers at the Si/SiO₂ interface: band-gap energy distribution, *J. Appl. Phys.* 56 (1984) 2844.
- [19] N.H. Thoan, et al., Interface state energy distribution and P_b defects at Si(110)/SiO₂ interfaces: comparison to (111) and (100) silicon orientations, *J. Appl. Phys.* 109 (2011) 013710.
- [20] V.V. Afanas'ev, Y.G. Fedorenko, A. Stesmans, Interface traps and dangling-bond defects in (100)Ge/HfO₂, *Appl. Phys. Lett.* 87 (2005) 032107.
- [21] M. Houssa, et al., Ge dangling bonds at the (100) Ge/GeO₂ interface and the viscoelastic properties of GeO₂, *Appl. Phys. Lett.* 93 (2008) 161909.
- [22] L. Soukup, et al., Germanium nitride layers prepared by supersonic r.f. plasma jet, *Surf. Coat. Technol.* 78 (1996) 280.
- [23] K. Mistry, et al., A 45 nm logic technology with high-k + metal gate transistors, strained silicon, 9 Cu interconnect layers, 193nm dry patterning, and 100% Pb-free packaging, 2007 IEEE Intl. Elec. Dev. Meeting, Washington, DC, 2007, pp. 247–250.
- [24] E.P. Gusev, et al., Ultrathin high-k metal oxides on silicon: processing, characterization and integration issues, *Microelectron. Eng.* 59 (2001) 341–349.
- [25] J.W. Zhang, et al., Microstructure optimization and optical and interfacial properties modulation of sputtering-derived HfO₂ thin films by TiO₂ incorporation, *J. Alloys Compd.* 611 (2014) 253–259.
- [26] L.Y. Huang, et al., Fabrication and characterization of La-doped HfO₂ gate dielectrics by metal-organic chemical vapor deposition, *Appl. Surf. Sci.* 256 (8) (2010) 2496–2499.
- [27] G. He, X. Chen, Z. Sun, Interface engineering and chemistry of Hf-based high-k dielectrics on III–V substrates, *Surf. Sci. Rep.* 68 (2013) 68–107.
- [28] G. He, et al., Modulating the interface quality and electrical properties of HfTiO/InGaAs gate stack by atomic-layer-deposition-derived Al₂O₃ passivation layer, *ACS Appl. Mater. Interfaces* 6 (2014) 22013–22025.
- [29] G. He, et al., Effect of dimethylaluminumhydride-derived aluminum oxynitride passivation layer on the interface chemistry and band alignment of HfTiO-InGaAs gate stacks, *APL Mater.* 1 (2013) 012104.
- [30] G. He, et al., Interface control and modification of band alignment and electrical properties of HfTiO/GaAs gate stacks by nitrogen incorporation, *J. Mater. Chem. C* 2 (2014) 5299–5308.
- [31] V. Chobpattana, et al., Nitrogen-passivated dielectric/InGaAs interfaces with sub-nm equivalent oxide thickness and low interface trap densities, *Appl. Phys. Lett.* 102 (2013) 022907.
- [32] Y. Saito, et al., Low-temperature formation of silicon nitride film by direct nitridation employing high-density and low-energy ion bombardment, *Jpn. J. Appl. Phys.* 38 (1) (1999) 2329–2332.
- [33] M. Edmonds, et al., Low-temperature thermal ALD of a SiN_x interfacial diffusion barrier and interface passivation layer on Si_xGe_{1-x}(001) and Si_xGe_{1-x}(110), *J. Chem. Phys.* 146 (2017) 052820.
- [34] M. Kavrik, et al., Ultralow defect density at sub-0.5nm HfO₂/SiGe interfaces via selective oxygen scavenging, *ACS Appl. Mater. Interfaces* 10 (2018) 30794–30802.
- [35] L. Zheng, et al., Improvement of Al₂O₃ films on graphene grown by atomic layer deposition with pre-H₂O treatment, *ACS Appl. Mater. Interfaces* 6 (2014) 7014–7019.
- [36] L. Zheng, et al., Property transformation of graphene with Al₂O₃ films deposited directly by atomic layer deposition, *Appl. Phys. Lett.* 104 (2014) 023112.
- [37] L. Zheng, et al., Semiconductor-like nanofilms assembled with AlN and TiN laminations for nearly ideal graphene-based heterojunction devices, *J. Mater. Chem. C* 4 (2016) 11067–11073.